

Supporting Information for

Driving magnetic domains at the nanoscale by interfacial strain- induced proximity

Ilya Valmianski¹, Arantxa Fraile Rodríguez^{2,3}, Javier Rodríguez-Álvarez^{2,3}, Montserrat García del Muro^{2,3}, Christian Wolowiec¹, Florian Kronast⁴, Juan Gabriel Ramírez⁵, Ivan K. Schuller¹, Amilcar Labarta^{2,3}, and Xavier Batlle^{2,3}*

¹ Department of Physics and Center for Advanced Nanoscience, University of California San Diego, La Jolla, CA 92093, USA

² Departament de Física de la Matèria Condensada, Universitat de Barcelona, 08028 Barcelona, Spain

³ Institut de Nanociència i Nanotecnologia (IN2UB), Universitat de Barcelona, 08028 Barcelona, Spain

⁴ Helmholtz-Zentrum Berlin für Materialien und Energie GmbH, 12489 Berlin, Germany

⁵ Department of Physics, Universidad de los Andes, Bogotá 111711, Colombia.

Table of contents	Page
• Figure S1. NEXAFS spectra around the L _{3,2} edges of Ni and V	2
• Figure S2. FMR contour plots above and below the V ₂ O ₃ SPT	3
• Figure S3. Magnetic hysteresis loops across the V ₂ O ₃ SPT	4
• Figure S4. Representative XMCD images corresponding to a second set of measurements	5
• Figure S5. Micromagnetic simulations performed using a distribution of anisotropy domains at each temperature that follows the experimental conductivity maps from Ref. 25	6
• Figure S6. Representative examples of experimental pair correlation curves obtained from the XMCD images	7

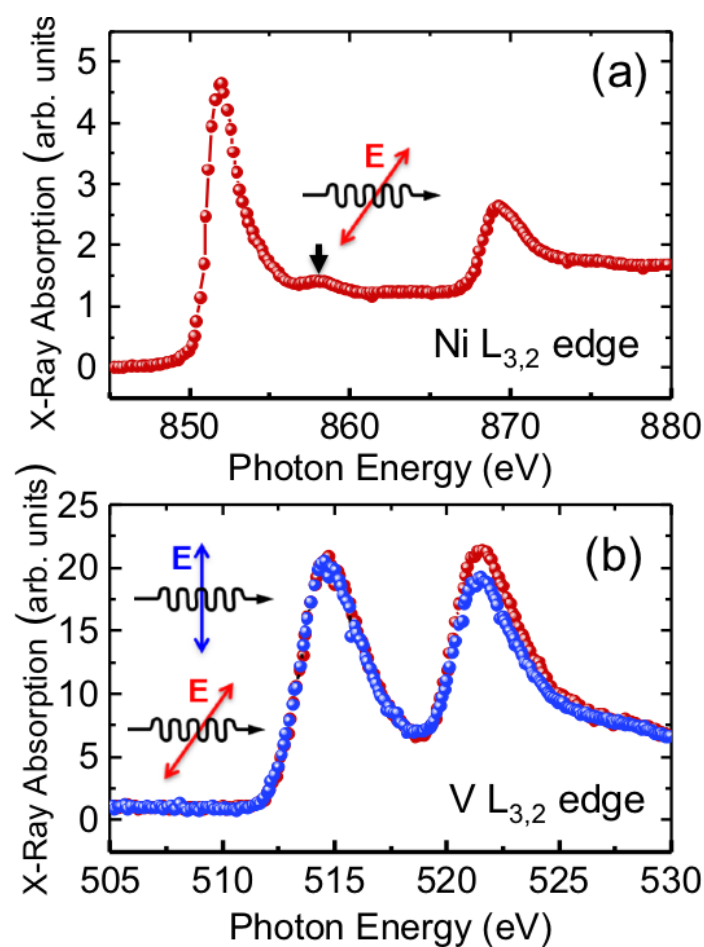


Figure S1. Near-Edge X-ray Absorption Spectroscopy (NEXAFS) recorded with linearly polarized X-rays around the $L_{3,2}$ edges of (a) Ni and (b) V. The red and blue curves are for electric field vector parallel and perpendicular to the surface plane, respectively. The presence of the expected satellite peak at about 6 eV above the L_3 edge, indicated by an arrow, as well as the absence of oxide-related multiplet features around the $L_{3,2}$ edges confirm the metallic character of the Ni film. (b) The multiplet structure related to the 2p-3d Coulomb interactions and crystal fields, often reported in vanadium oxides^{14, 36}, is not apparent from our spectra, possibly due to a limited energy resolution (<0.5 eV) and the effect of sample charging on our secondary electron yield measurements that may broaden the main peaks and smear out shoulder features.

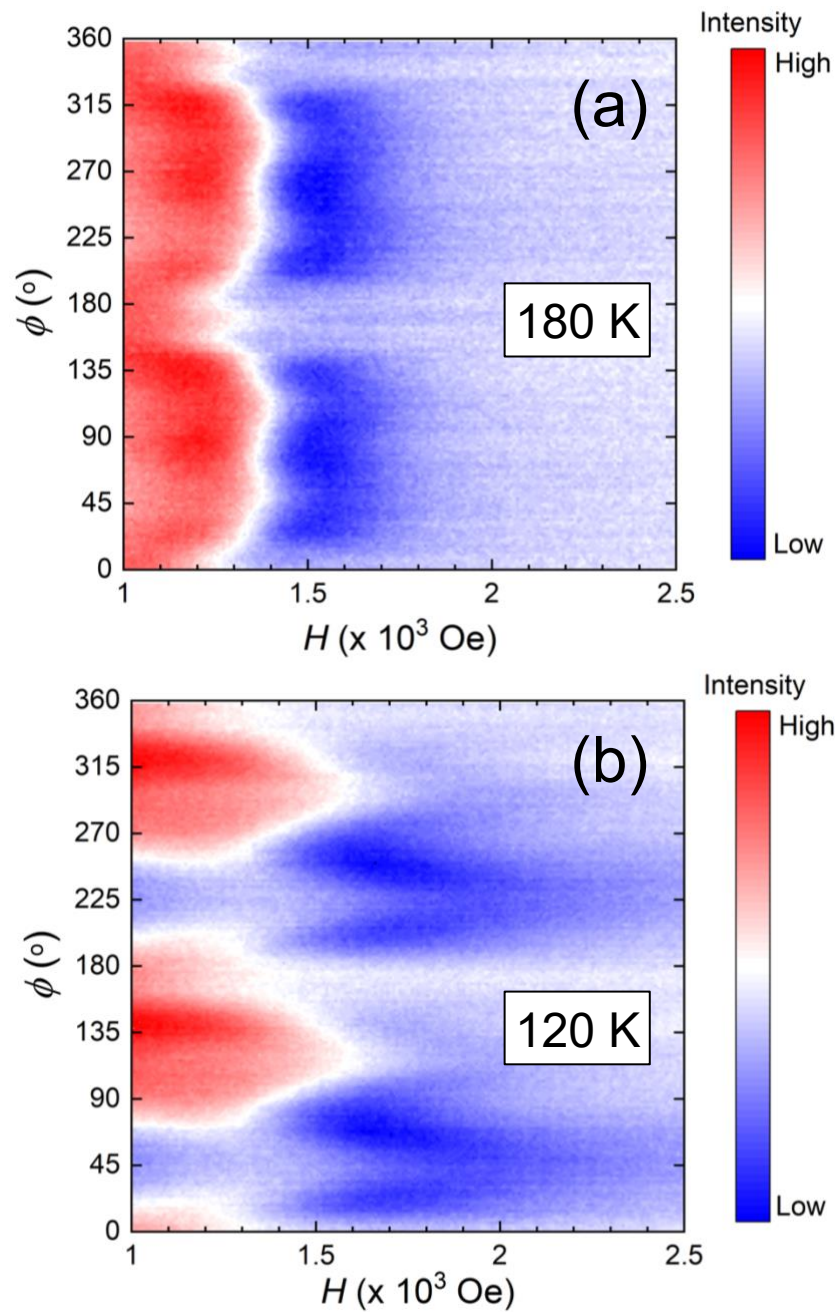


Figure S2. (a) Angular dependence of ferromagnetic resonance (FMR) as a function of dc magnetic field above the structural phase transition (SPT) at 180 K in Ni/V₂O₃ and (b) below the SPT at 120 K. The initial 0° angle is set along the (0 1 -5)_{RH} direction.

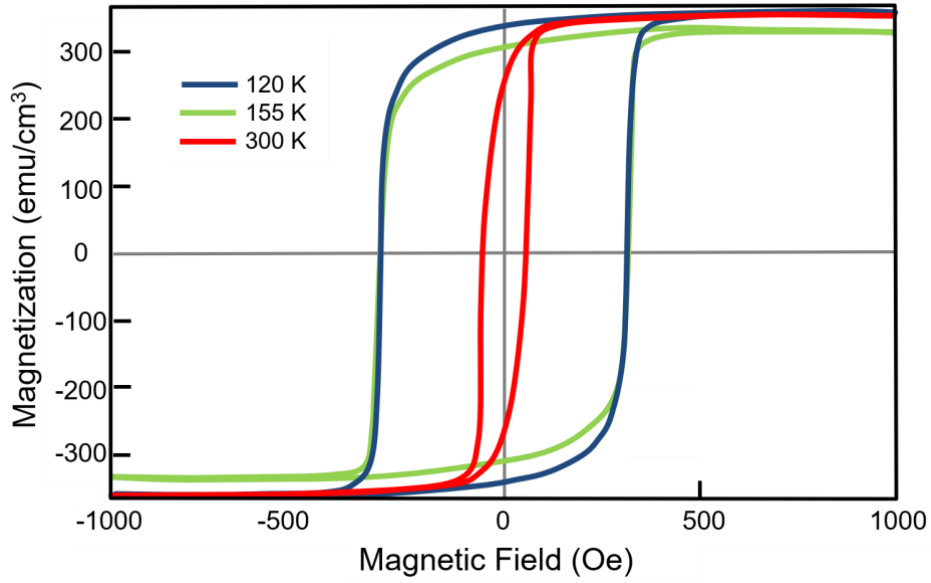


Figure S3. Magnetic hysteresis loops of Ni(10 nm)/V₂O₃(100 nm) with the magnetization normalized by the Ni volume for three selected temperatures across the V₂O₃ structural phase transition: above (300 K, red), in the middle (155 K, green), and below (120 K, blue) the SPT of V₂O₃. Data were collected with the magnetic field applied along a direction forming an angle of 45° with the high-temperature Ni easy axis, n_H ((0 1 -5)_{RH} direction) (see Fig. 1d).

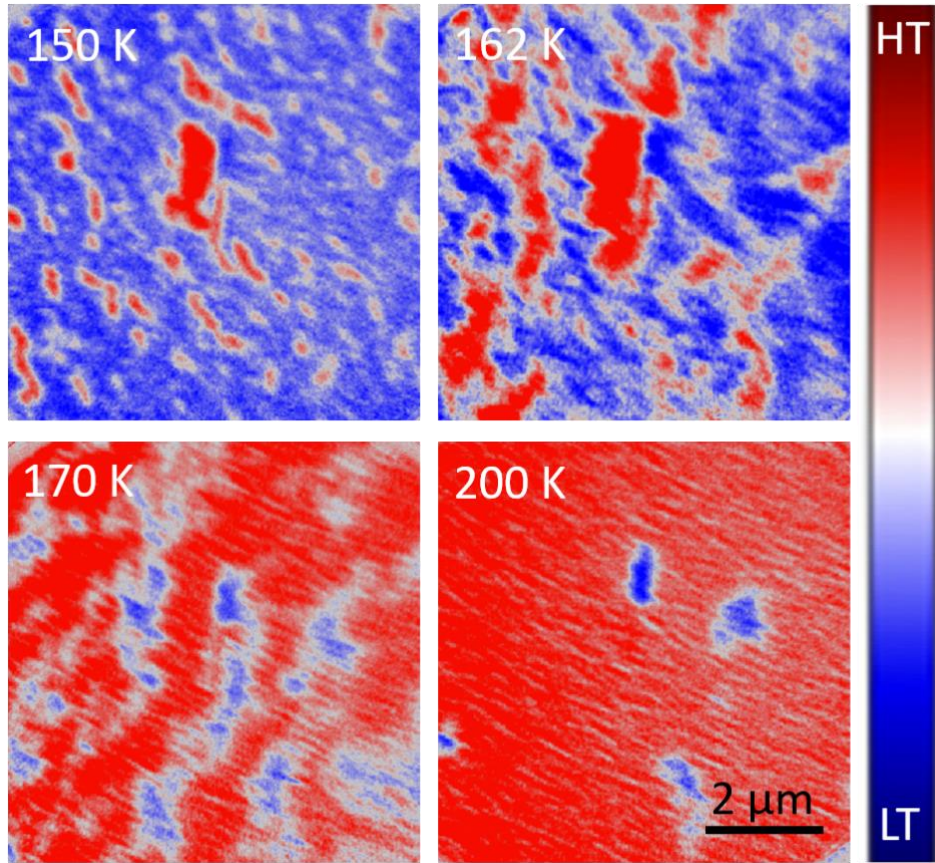


Figure S4. (a) Representative XMCD images corresponding to a second set of measurements (so called cycle 2 in the main text) at temperatures below (150 K), across (162 K, 170 K) and above (200 K) the structural phase transition of V_2O_3 . The images were recorded in the same area of the sample and following the same experimental protocol as for the images shown in Fig. 3. The nucleation and growth of magnetic domains in cycle 2 occurs in different places and following a different sequence as those in cycle 1 (Fig. 3), thus showing a stochastic domain nucleation process across the SPT and a non-appreciable number of pinning centers.

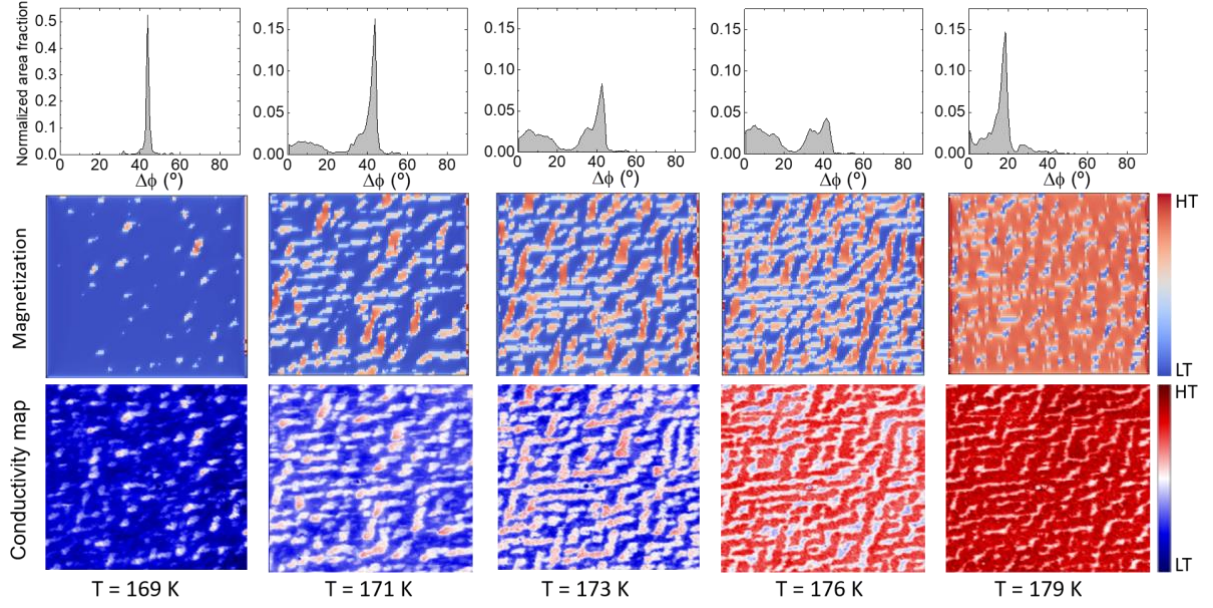


Figure S5. Results of micromagnetic simulations as a function of the temperature showing histograms of the average rotation angle of the Ni magnetization, $\Delta\phi$ (top row panels), the experimental spatial distribution of the magnetization angle (middle row panels) and the experimental spatial distribution of the low-temperature insulating and high-temperature metallic phases taken from Ref. 25 in a V_2O_3 film similar to that in our sample (bottom row panels). In this case, the simulations were performed following the same procedure as in Fig. 5 but with a distribution of anisotropy domains at each temperature that follows the experimental conductivity maps²⁵. In the middle row panels, the regions with orientations of the Ni magnetization corresponding to the high- and low-temperature phases are colored in red and blue, respectively. In the bottom row panels, the blue/red colored areas correspond to insulating/metallic regions, respectively in V_2O_3 . The high resemblance between the local patterns in the Ni magnetization and those of the V_2O_3 conductivity at the same temperature is a clear indication that the main source of the effective uniaxial anisotropy axes arises from strain induced by the proximal V_2O_3 layer across the SPT.

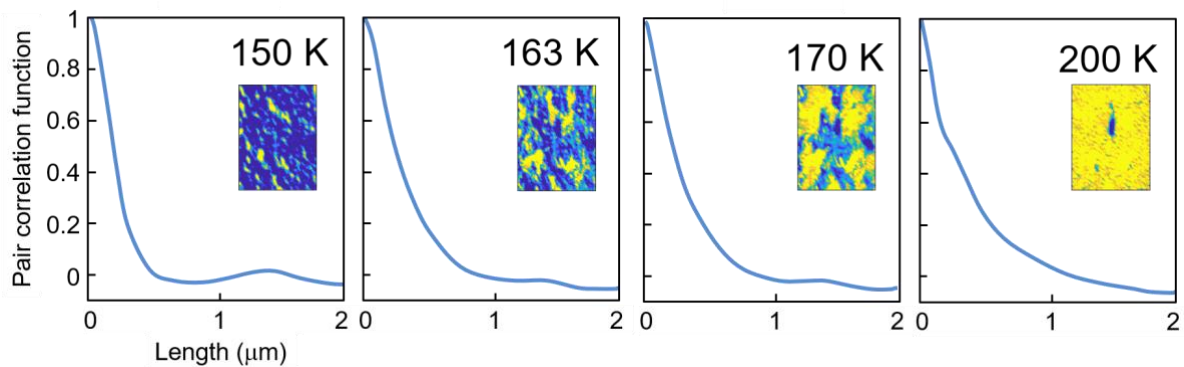


Figure S6. Representative examples of pair correlation curves quantified from the XMCD images shown in the insets, corresponding to a Ni (10 nm)/V₂O₃ (100 nm) sample (right). The domain correlation lengths shown in Fig. 6a were computed from fits of such experimental pair correlation curves to a single exponential decay.